

Polymer Chemistry

Accepted Manuscript



This is an *Accepted Manuscript*, which has been through the Royal Society of Chemistry peer review process and has been accepted for publication.

Accepted Manuscripts are published online shortly after acceptance, before technical editing, formatting and proof reading. Using this free service, authors can make their results available to the community, in citable form, before we publish the edited article. We will replace this *Accepted Manuscript* with the edited and formatted *Advance Article* as soon as it is available.

You can find more information about *Accepted Manuscripts* in the [Information for Authors](#).

Please note that technical editing may introduce minor changes to the text and/or graphics, which may alter content. The journal's standard [Terms & Conditions](#) and the [Ethical guidelines](#) still apply. In no event shall the Royal Society of Chemistry be held responsible for any errors or omissions in this *Accepted Manuscript* or any consequences arising from the use of any information it contains.

Reaction Mechanism and Synergistic Anticorrosion Property of Reactive Blends of Maleimide-Containing Benzoxazine and Amine-Capped Aniline Trimer

Shin-Chen Lin¹, Chuan-Shao Wu², Jui-Ming Yeh³, Ying-Ling Liu^{1*}

1. Department of Chemical Engineering, National Tsing Hua University, Hsinchu 30013, Taiwan

2. Department of Materials and Fiber & Graduate School of Materials Applied Technology, Taoyuan Institute of Innovation Technology, Chungli, Taoyuan 32091, Taiwan

3 Department of Chemistry and Center for Nanotechnology, Chung Yuan Christian University, Chungli, Taoyuan 32023, Taiwan

*Corresponding to Professor Ying-Ling Liu, E-mail: liuyl@mx.nthu.edu.tw; Tel: +886-3-5711450; Fax: +886-3-5715408

Abstract

This work studies the reaction mechanism and properties of reactive blends possessing a maleimide-containing benzoxazine compound (MI-Bz) and an amine-capped aniline trimer (ACAT). For the blends of MI-Bz and ACAT under a thermal process, the quinoid reaction of ACAT performs first at about 96 °C and the Michael addition reaction between the amine groups of ACAT and the maleimide group of MI-Bz follows at high temperatures. The amine group of ACAT catalyzes the ring-opening reaction of benzoxazine groups of MI-Bz. The active species in the ring-opening reaction of benzoxazine groups are reactive toward the amine groups of ACAT. These two reactions build up the covalent bonding between ACAT and MI-Bz compounds. The thermally-cured MI-Bz/ACAT mixtures (CR-MI-Bz/ACAT) demonstrate good thermal stability, high flame retardancy, and a synergistic effect on anticorrosion property. The water resistance (from MI-Bz) and the electroactivity (from ACAT) of the CR-MI-Bz/ACAT materials contribute to their high anticorrosion efficiency. The sample possessing 33 wt% ACAT shows a protection efficiency of 98% and a corrosion rate of $4.8 \mu\text{m y}^{-1}$ for cold-rolled steel substrate, which is about one order lower than that recorded with the neat ACAT sample.

KEYWORDS benzoxazine; aniline trimer; crosslinking; anticorrosion; thermosets

1. Introduction

Benzoxazine compounds, which are prepared with various and inexpensive raw materials, could perform thermally-activated ring-opening polymerization to result in the corresponding polybenzoxazines.^{1,2} Basing on their great molecular design flexibility and unique properties, benzoxazine compounds and their corresponding polymers have received massive research activities at both academic and industrial sides. With the concepts of molecular designs for benzoxazine compounds, one effective approach to improve the properties of polybenzoxazines is introduction of another functional group to the structure of benzoxazine compounds.³⁻¹² Incorporation of another polymerizable group to benzoxazine compounds could increase the crosslinking densities and the glass transition temperatures (T_g) of the corresponding polybenzoxazines.¹³⁻¹⁶ Phosphorylation of benzoxazines improves the flame retardancy of the corresponding polymers.¹⁶⁻¹⁹ The benzoxazines possessing hydroxyl^{20,21} and carboxylic acid^{22,23} groups exhibit relatively low polymerization temperatures and good processing property. Moreover, copolymerization of benzoxazines with another reactive compound is also a convenient approach for property modification of polybenzoxazines. The ring-opening polymerization of benzoxazines generates phenol groups which are highly reactive toward many chemical groups. As a result, benzoxazine compounds are effective components to prepare reactive blends with other chemicals such as epoxy,²⁴ isocyanate,²⁵ maleimide,^{26,27} and cyanate ester.^{28,29} The active intermediates in the ring-opening polymerization of benzoxazines are also highly reactive toward thiol,³⁰ primary amine,³¹ and active aromatic groups.^{3,32,33} The reaction has been applied to utilize benzoxazine compounds as crosslinking agents for linear polymers such as chitosan³¹ and polybenzimidazole (PBI).^{32,33} The reaction diversity of benzoxazine compounds and the attractive properties of the corresponding polymers significantly extends

their scopes and fields of application. Crosslinked resins of benzoxazine and cyanate ester have shown low dielectric constants for microelectronic dielectrics.²⁹ Polybenzoxazine-crosslinked PBI polymers show application potential as proton exchange membranes for fuel cells.^{32,33}

Polybenzoxazines possess hydrogen bonding in various types. The interaction of hydrogen bonding results in the extremely low surface-free-energy (SFE) of polybenzoxazines down to about 16.4 mJ m^{-2} ,³⁴ which is even lower than the value (20 mJ m^{-2}) recorded with poly(tetrafluoroethylene). Basing on the low SFE, polybenzoxazines are suitable materials for preparation of superhydrophobic,³⁵ anti-biofouling,³⁶ and anticorrosion materials.^{37,38} Zhou and coworkers³⁷ reported that silane-functionalized polybenzoxazine is an effective anticorrosive coating material with superior adhesion ability to the metal substrates. The high hydrophobicity, low water uptakes, and high water resistance of the polybenzoxazine contribute to their high anticorrosion efficiency. Blends of the silane-functionalized polybenzoxazine with epoxy resins improve the anticorrosion property of epoxy protective coatings with a high protection efficiency above 98%.³⁸ The anticorrosion efficiency increases with increasing the contents of the polybenzoxazines in the benzoxazine/epoxy blends.

Polyaniline (PANI) is a conducting polymer and has shown ability to perform better anticorrosion action on substrates than some polymers.³⁹ The electroactivity of PANI induces the formation of protective passive oxide layer covering on the substrates to perform the anticorrosion effect.⁴⁰ Moreover, polymers prepared from amine-capped aniline pentamer and trimer also exhibit similar electroactivity. As a result, Yeh and coworkers⁴¹ demonstrated that incorporation of amine-capped aniline trimer (ACAT) segments into the structures of polyimides could effectively increase the anticorrosion protection effect of polyimides. Reactive blends of ACAT and epoxy resins also showed electroactive characteristics and anticorrosion property.⁴²

The sample containing 40 mol% ACAT exhibited a protection efficiency of 65%, which was much higher than the value of 10% recorded with the neat epoxy resin. Further studies revealed that fabrication of PANI into a superhydrophobic structure could further enhance the anticorrosion efficiency.⁴³ Nevertheless, the approach involved complicated processing procedure and the obtained materials suffered with the poor stability of the structure surface.

The above discussion suggests (1) studies on the reaction route of benzoxazine-based reactive blends are attractive for understanding the structure and property of the resulting polymers, (2) increase in the hydrophobicity of PANI-based polymers might improve the anticorrosion efficiency, and (3) the low SPE benzoxazine-based polymers could be suitable agents working together with PANI for anticorrosion application. Therefore, this work studies the reactive blends of a maleimide-containing benzoxazine (MI-Bz)¹³ and ACAT (Figure 1). The reaction mechanism between the two compounds under the thermally curing process is examined with Fourier transform infrared spectroscopy (FTIR) and differential scanning calorimetry (DSC). Moreover, the two compounds have shown a synergistic effect on anticorrosion property. The cured MI-Bz/ACAT blending sample containing 33 wt% of ACAT shows a corrosion rate of $4.8 \mu\text{m y}^{-1}$ and a protection efficiency of 98.0%, both are superior over the data recorded with the neat MI-Bz and ACAT samples.

2. Experimental

2.1. Materials

MI-Bz was prepared in the laboratory according to the reported method¹³ using 4-maleimidophenol, aniline, and formaldehyde as raw materials. 4-Maleimidophenol was prepared with the reported method.⁴⁴ Aniline and formaldehyde were purchased from Acros Chemical Co. and used as received. Preparation of ACAT was conducted with the oxidative coupling reaction

between 1,4-phenylenediamine (Aldrich Chem. Co.) and aniline using ammonium persulfate (Aldrich Chem. Co.) as an oxidant.⁴⁵ The aniline used in the reaction was distilled prior to use. Reagent grade solvents have been employed for the reaction and sample preparation.

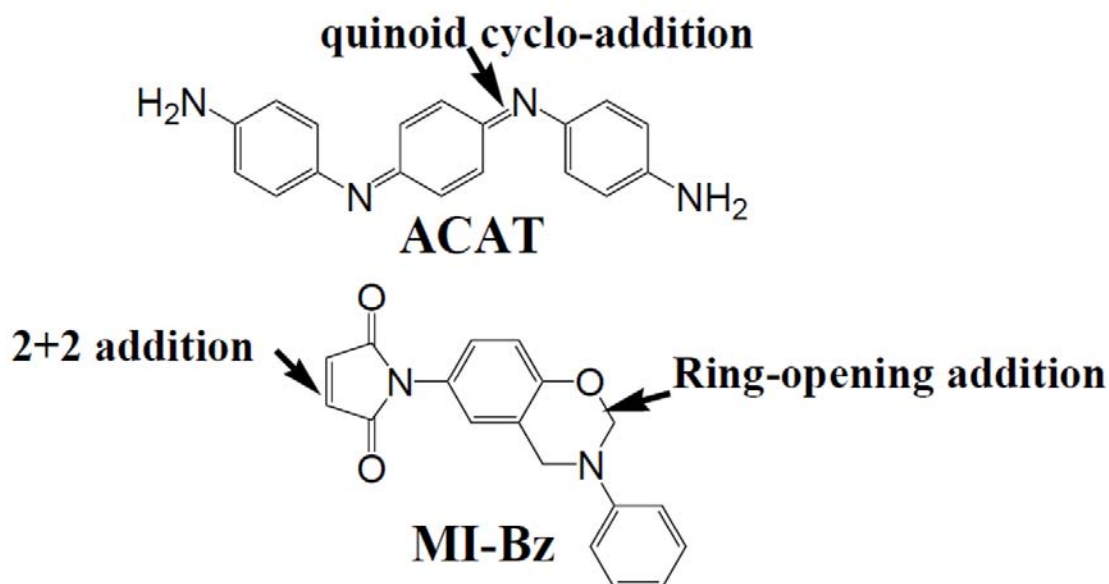


Figure 1. Chemical structures and thermally-induced reactions of ACAT and MI-Bz.

2.2. Measurements

Transmission FTIR spectra were recorded with a Perkin Elmer Spectrum II FTIR instrument equipped with a temperature-controlled heating stage. Reflectance FTIR measurements were conducted with the same FTIR instrument equipped with a multiple internal reflectance apparatus and a ZnSe prism as an internal reflection element using attenuated total reflectance (ATR) method. DSC thermograms were recorded with a Thermal Analysis (TA) Diamond DSC instrument at a heating rate of 10 °C min⁻¹ and under a nitrogen gas flow of 50 mL min⁻¹. Dynamic mechanical analysis (DMA) was conducted with a TA Q800 DMA instrument at a frequency of 1 Hz and a heating rate of 5 °C min⁻¹. A three-point-bending model

was employed. Thermogravimetric analysis (TGA) was performed with a TA STD Q600 instrument at a heating rate of $10\text{ }^{\circ}\text{C min}^{-1}$ and under a nitrogen gas flow of 80 mL min^{-1} . Scanning electron microscopy (SEM) observation were performed with a Hitachi S-4800 field-emission SEM. Cyclic voltammetry measurements were carried out with an VoltaLab-PST050 instrument using saturated calomel electrode (SEC) as the reference electrode and a carbon rode as the counter electrode. Electrochemical impedance spectroscopy (EIS) curves were recorded with an AutoLab FRA2 instrument.

2.3. Preparation of crosslinked MI-Bz/ACAT samples

MI-Bz and ACAT in a certain weight ratio were dissolved in 1-methyl-2-pyrrolidone (NMP) in a concentration of 0.5 mg mL^{-1} . The solution was treated with an ultrasonic bath for 1 h, poured into a Teflon-lining stainless mold, and then thermally cured at $130\text{ }^{\circ}\text{C}$ for 1 h, $200\text{ }^{\circ}\text{C}$, for 1 h, and $250\text{ }^{\circ}\text{C}$ for 1 h. The samples have been coded as CR-MI-Bz/ACAT-X, where X denotes to the weight percentage of ACAT in the curing composition. The samples were used for TGA and DMA measurements.

2.4. Water absorption measurements

The dry sample was weighted to be W_d and immersed in The membrane was immersed in a $3.5\text{ wt}\%$ $\text{NaCl}_{(\text{aq})}$ solution. The sample was draw out, swept with a cleaning paper, and then weighted at a certain period of time to give $W_{w,t}$. The water uptake of the sample at time t is determined by $(W_{w,t} - W_d) * 100\%$.

2.5. Anticorrosion property measurements

Cold-rolled steel (CRS) pieces in $1.2\text{ cm} * 1.5\text{ cm}$ were polished and washed with methanol and acetone using an ultrasonic bath. The NMP solution of MI-Bz and ACAT (in a certain weight ratio) with a concentration of 0.5 mg mL^{-1} was dropped on the surface of steel pieces.

The steel pieces were then put in an oven to thermally cure the MI-Bz/ACAT mixtures at 130 °C for 1 h, 200 °C, for 1 h, and 250 °C for 1 h. The obtained samples were applied for anticorrosion tests. The cyclic voltammetric measurements were taken from -1.1 to 0 V at a scan rate of 100 mV min⁻¹. For polarization current experiments, the open circuit potential (OCP) vs SCE at equilibrium state is recorded as the corrosion potential (E_{corr}). The scanning range of potential is from 500 mV below to 500 mV above the E_{corr} at a scan rate of 100 mV min⁻¹. The tests were performed with a 3.5 wt% NaCl(aq) as a corrosive medium. EIS curves were performed in a frequency range from 100 kHz to 10 MHz and a 3.5 wt% NaCl(aq) solution as an electrolyte.

3. Results and discussion

3.1. Reactions of MI-Bz/ACAT blends

Both MI-Bz and ACAT could undergo thermally-induced polymerization (Figure 1). As shown in the DSC thermograms (Figure 2), pure ACAT exhibits two exothermic peaks at 96 and 182 °C. The polymerization behaviors of MI-Bz result in the exothermic peaks at 205 and 248 °C. The blends of these two compounds (MI-Bz/ACAT-X, where X denotes to the percentage of ACAT of the curing composition) show very different DSC thermograms compared to the thermograms recorded with the individual neat compounds. The exothermic peak at about 96 °C which associates to the reaction of ACAT portion appears obviously in the DSC thermograms of the blends possessing ACAT contents higher than 10 wt%. The intensity of the peak at temperatures above 200 °C, which associates to the MI-Bz polymerization, decreases with increasing the ACAT contents. This exothermic behavior almost disappears for the samples possessing high ACAT contents. Meanwhile, the blends show an exothermic peak at about 112 °C which does not appear in the thermogram of the neat MI-Bz and ACAT compounds. The result might indicate that some interactions between these two compounds occur in the thermal process. The

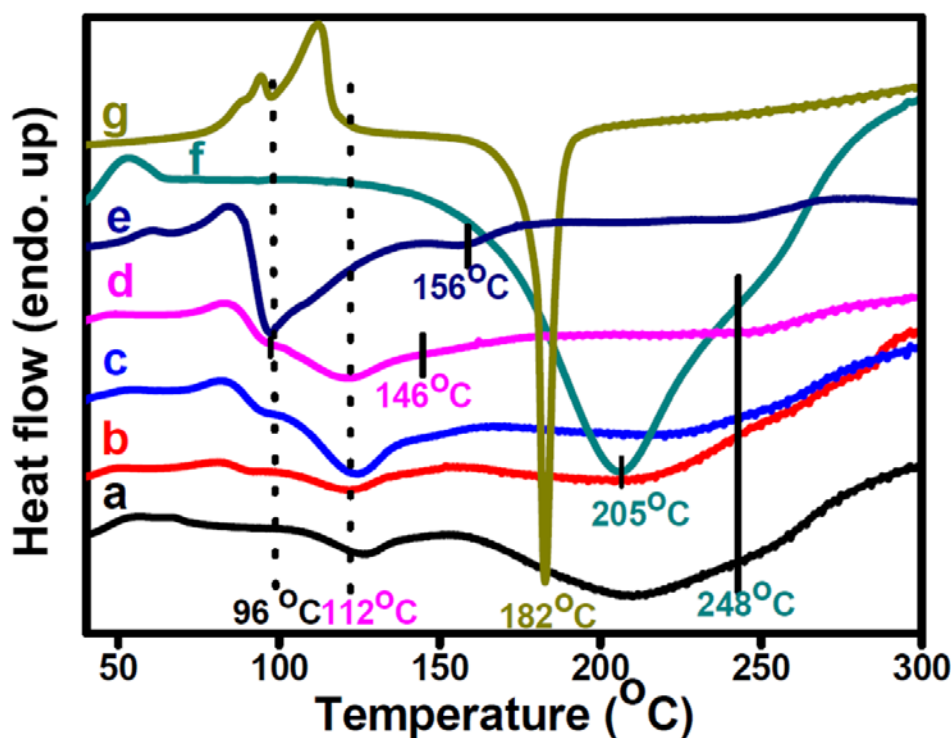


Figure 2. DSC thermograms recorded on (a) MI-Bz/ACAT-5, (b) MI-Bz/ACAT-10, (c) MI-Bz/ACAT-20, (d) MI-Bz/ACAT-33, (e) MI-Bz/ACAT-50, (f) neat MI-Bz, and (g) neat ACAT samples.

reactions associating to the exothermic behaviors of the samples have been traced with temperature-dependent FTIR spectra. As discussed in the literature,⁴⁶ the absorption peak at 1600 cm^{-1} in the FTIR spectrum of ACAT associates to the stretching vibration of quinoid rings. The intensity of the peak decreases gradually in the temperatures between 90-130 $^{\circ}\text{C}$. The peaks at 3201 and 3308 cm^{-1} , which associate to the vibration of amine groups, almost disappear in the FTIR spectra recorded at temperatures above 200 $^{\circ}\text{C}$. As a result, the second exothermic peak in the DSC thermogram of ACAT might associate with the polymerization of aniline groups. It is noteworthy that small amount (5 wt%) of ACAT is enough to alter the reaction route of MI-Bz

as a new exothermic peak at about 112 °C appears in the DSC thermograms of the blends of MI-Bz and ACAT. The peak becomes predominant for the samples of MI-Bz/ACAT-25 and MI-Bz/ACAT-33. The temperature-dependent FTIR spectra have been recorded with MI-Bz/ACAT-33 to trace the reactions associating to the exothermic peak at 112 °C (Figure 3a). First, the intensity of the peaks at 1600 cm⁻¹ decreases at 90-110 °C to imply the performance of the quinoid ring reaction at the temperature region. As a result, the exothermic peak at 96 °C in the DSC thermogram of MI-Bz/ACAT-33 corresponds to the quinoid ring reaction. The peak intensity of the amine groups of ACAT decreases at about 110 °C and disappears at 150 °C. As the polymerization of aniline groups of ACAT occurs at temperatures above 200 °C, the disappearance of the amine absorption at the relatively low temperatures might indicate the occurrence of the Michael addition reaction between the amine groups of ACAT and the maleimide groups of MI-Bz. The decrease in the peak intensity of C-N-C linkage of maleimide group at 1146 cm⁻¹ and the appearance of the C-N-C linkage of succimide group at 1178 cm⁻¹ provide further supports to the performance of the Michael addition.⁴⁷ The peak intensity of amine groups further decrease at 150-170 °C. Meanwhile, the absorptions of the ring structure of benzoxazine group at 935 and 1235 cm⁻¹ also decrease in the peak intensity at the temperatures region, indicating the performance of the ring-opening reaction benzoxazine groups. As a result, the amine group of ACAT might involve in the ring-opening reaction of the benzoxazine groups to reduce the reaction temperature from about 250 to 170 °C. Alhwaige *et al.*³¹ reported that the amine groups of chitosan might catalyze the ring-opening addition reaction and involve in the ring-opening reaction of benzoxazine groups by an oxygen protonation mechanism. This reaction mechanism could be applied to the above-mentioned reactions between MI-Bz and ACAT. The occurrence of Michael addition and benzoxazine ring-opening reactions at the relatively low

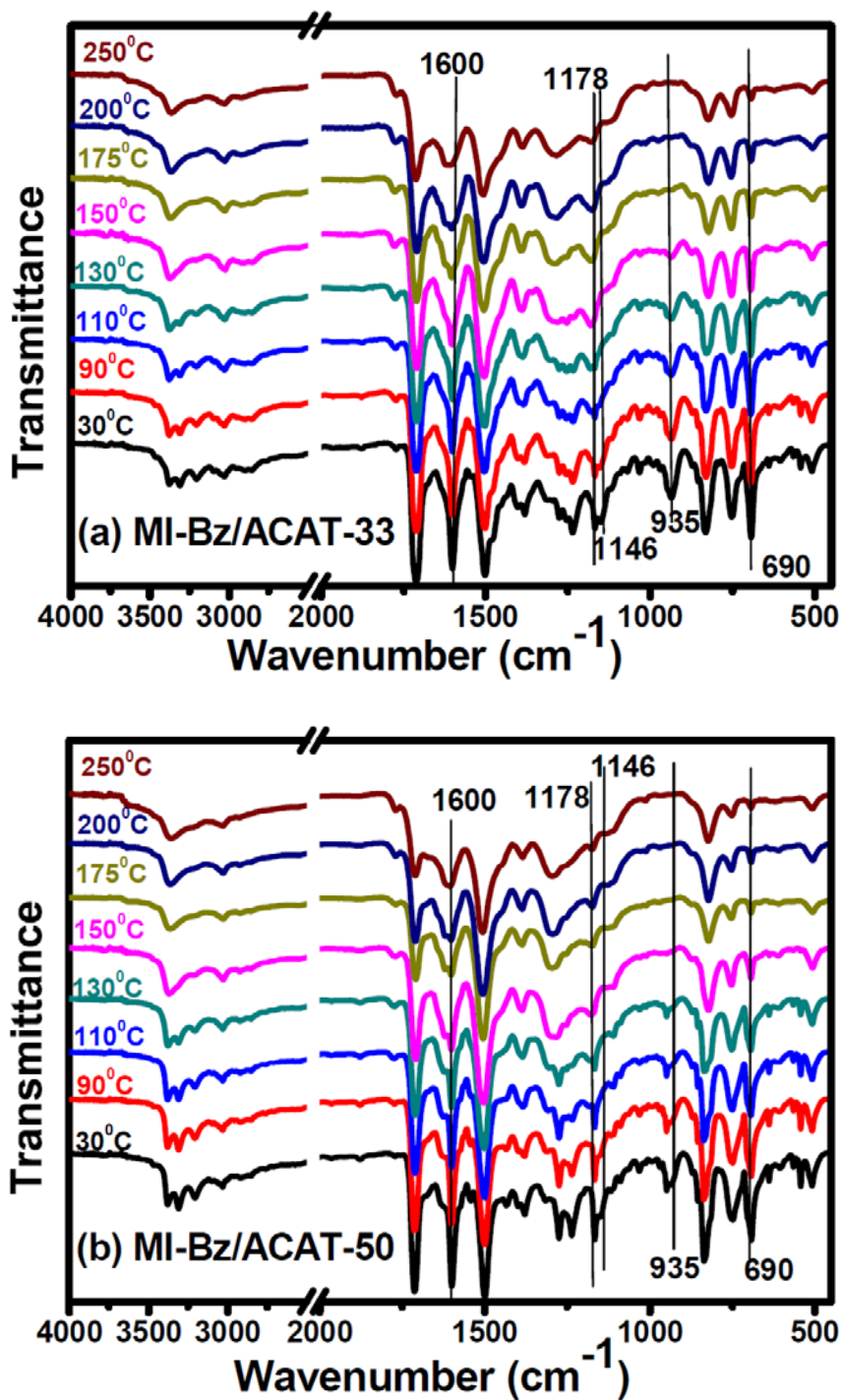


Figure 3. Temperature-dependent FTIR spectra recorded on (a) MI-Bz/ACAT-33 and (b) MI-Bz/ACAT-50 at the heating process.

temperature region, compared to the neat MI-Bz compound, results in the disappearance of the exothermic peaks at temperatures above 200 °C in the DSC thermogram of MI-Bz/ACAT-33. Moreover, the temperature-dependent FTIR spectra of MI-Bz/ACAT-50 reveal similar results discussed with MI-Bz/ACAT-33 (Figure 3b). Nevertheless, the large amount of ACAT in the curing composition results in the relatively predominant exothermic peak of quinoid ring reaction. For MI-Bz/ACAT-50, the absorption of the amine group of ACAT could be still observed in the FTIR spectrum recorded at 150 °C due to the excess ACAT in the curing composition, although this peak almost disappears in the FTIR spectrum of MI-Bz/ACAT-33 at 150 °C. The residual amine groups might perform self-polymerization to form polyaniline structure. The aniline polymerization reaction contributes to the exothermic peak at 156 °C in the DSC thermogram of MI-Bz/ACAT-50. Nevertheless, the temperature of aniline polymerization observed for MI-Bz/ACAT-50 is a little lower than that for the neat ACAT.

Basing on the results discussed above, a reaction mechanism for the MI-Bz/ACAT blends is proposed (Figure 4). ACAT performs the quinoid reaction first at about 96 °C. The Michael addition reaction between the amine groups of ACAT and the maleimide group of MI-Bz occurs after the quinoid reaction.⁴⁷ Meanwhile, the amine groups of ACAT protonate the oxygen atom of the benzoxazine groups to induce the ring-opening reaction of benzoxazine groups so as to generate iminium ion active species. The iminium species are reactive toward both the benzoxazine ring of MI-Bz and the amine groups of ACAT. The reaction between the iminium active species and benzoxazine ring performs the common polymerization route for benzoxazines,³¹ and the reaction between the iminium active species and the amine groups of ACAT builds up covalent linkages between ACAT and MI-Bz networks.³¹ The Michael addition reaction between the maleimide group of MI-Bz and the amine groups of ACAT also contribute

to build the covalent linkages between ACAT- and MI-Bz-based networks. As a result, the obtained CR-MI-Bz/ACAT-X samples possess polymeric networks comprising of ACAT and MI-Bz structures rather than interpenetrating networks of these two compounds.

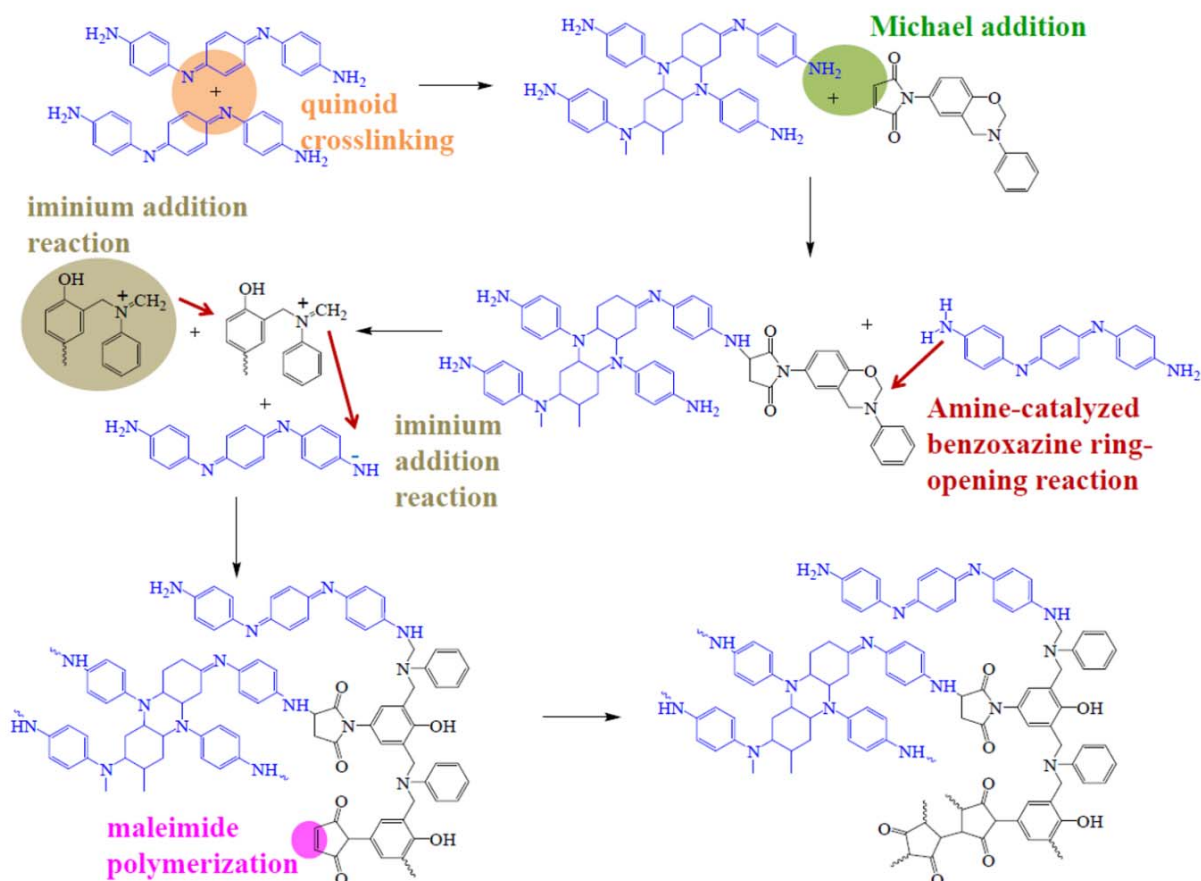


Figure 4. The reaction mechanism proposed for the thermally-induced curing reactions of MI-Bz/ACAT blends.

3.2. Thermal properties of CR- CR-MI-Bz/ACAT-X samples

The CR-MI-Bz/ACAT-X samples possess polyaniline and polybenzoxazine crosslinked structures. Figure 5 shows the DMA thermograms of the CR-MI-Bz/ACAT-X samples. All the samples exhibit high storage modulus of about 3.0 GPa at 50 oC, which is a little higher than the

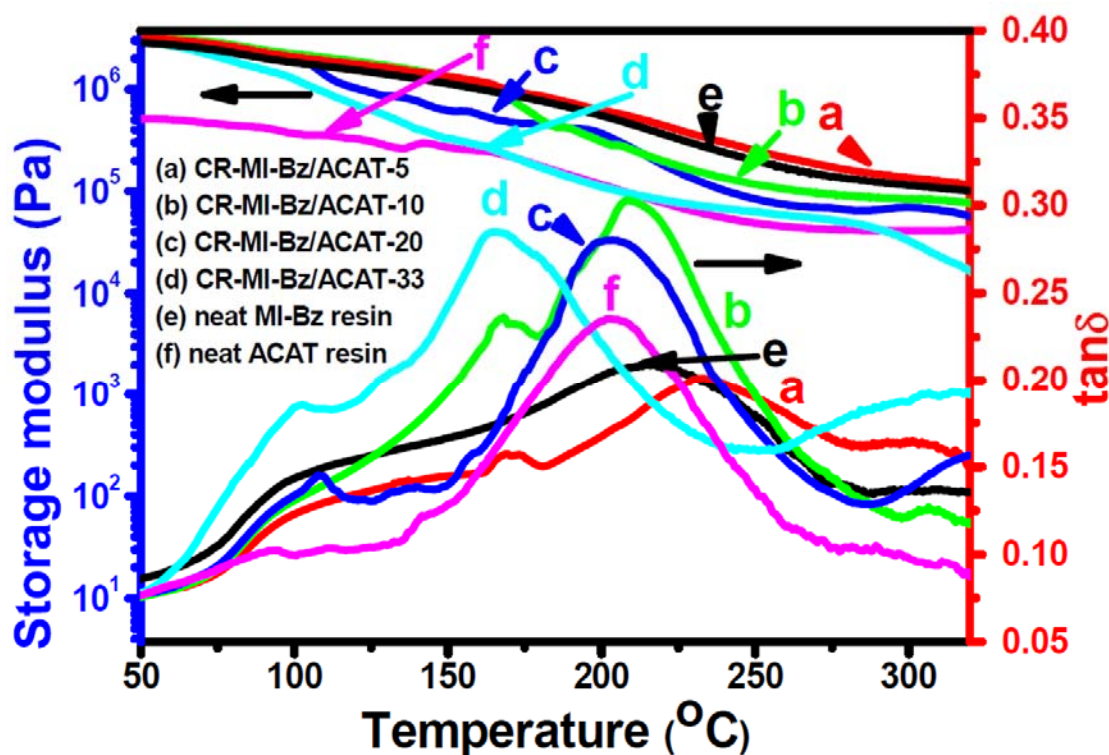


Figure 5. DMA thermograms recorded on the thermally-cured resins of MI-Bz, ACAT, and their reactive blends.

value (about 2.8 GPa) recorded with the neat CR-MI-Bz sample. It is noteworthy that the storage modulus of the CR-MI-Bz/ACAT-X samples is much superior over that recorded with the neat ACAT sample (about 0.5 GPa). The glass transition temperatures (T_g) of the tested samples recorded with the peak of the $\tan\delta$ curves are collected in Table 1. Addition small amount (5 wt%) of ACAT to MI-Bz results in an increase in the T_g from 215 to 233 °C as the result observed for MI-Bz/ACAT-5. The increased T_g could be attributed to the hydrogen bonding between the amine groups of ACAT and the carbonyl and hydroxyl groups of MI-Bz. The T_g 's of the CR-MI-Bz/ACAT-X samples which possess ACAT contents above 5 wt% are smaller than the T_g of the neat MI-Bz resin, as the neat ACAT resin shows a relatively low T_g . It is

noteworthy that the T_g of the CR-MI-Bz/ACAT-33 sample is much lower than the values recorded with the two neat MI-Bz and ACAT resins, due to the rapid decrease in the storage modulus appearing at the low-temperature region. The values of the storage modulus at the rubbery state, corresponding to the crosslinking density, of the samples show an order same as the order of their T_g 's. CR-MI-Bz/ACAT-5 has the highest crosslinking density ($11.8 \text{ mmol cm}^{-3}$) among the samples. Figure 6 shows the TGA thermograms of the CR-MI-Bz/ACAT-X samples. Although the thermal stability of the co-cured samples are not as high as that observed with the neat resins, all the CR-MI-Bz/ACAT-X samples exhibit good thermal stability (the temperatures at 5 wt% loss) above $320 \text{ }^\circ\text{C}$ (Table 1). It is noteworthy that the order of the thermal stability of the co-cured samples is still same as the order of their T_g 's and crosslinking densities. The decreased thermal stability of the co-cured samples might be attributed to the relatively thermally-unstable C-N linkages formed with the Michael addition reaction between the maleimide group of MI-Bz and the amine group of ACAT. All the samples exhibit high char yields at $800 \text{ }^\circ\text{C}$ above 50 wt%. The higher the char yield is, the smaller amount of combustible degraded products is released to the gaseous phase while the samples under flame. The van Krevelen equation gives the relationship between the char yield and the flame retardancy of a polymer as⁴⁸

$$\text{LOI}=17.5+0.4\text{CR}$$

, where LOI is the limited oxygen index and CR is the char yield at $800 \text{ }^\circ\text{C}$. As a result, the LOI values of the CR-MI-Bz/ACAT-X resins have been calculated to be 38-40. The high LOI values imply the high flame retardancy of the CR-MI-Bz/ACAT-X resins to demonstrate self-extinguishing property. Addition of flame retardants is not necessary for the resins for general applications.

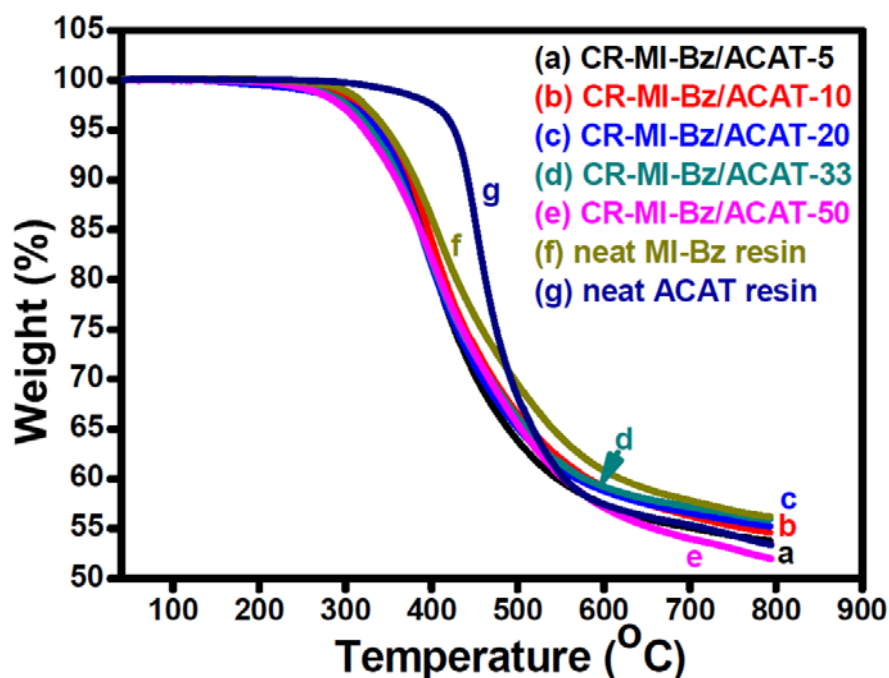


Figure 6. TGA thermograms recorded on the thermally-cured resins of MI-Bz, ACAT, and their reactive blends.

3.3. Synergistic effect of ACAT and MI-Bz on anticorrosion property

The CR-MI-Bz/ACAT-X samples have been coated on CRS plates for the anticorrosion property measurements. The Tafel plots obtained with the samples are shown in Figure 7a. With the Tafel plots, the corrosion potential (E_{corr}) and corrosion current (I_{corr}) have been obtained by the extrapolation method.⁴⁹ Consequently, the corrosion rate and protection efficiency could be calculated with the data of E_{corr} and I_{corr} for quantitative evaluation of the anticorrosion performance (Table 2).⁴⁹ The bare steel shows an E_{corr} of about -892 mV, which has been improved to -800 and -685 mV while being coated with the cured neat MI-Bz and neat ACAT resin, respectively. The result suggests that ACAT has a better anticorrosion property than does MI-Bz for steel. The same result has also been supported with the recorded values of I_{corr} .

Coating ACAT or MI-Bz on steel plates significantly reduces its I_{corr} value from 12.25 to about 1.80-1.96 $\mu\text{A cm}^{-2}$. The protection efficiency calculated for both ACAT and MI-Bz is about 85%, which is close to the value reported to an epoxy resin.⁴⁹ It is noteworthy that the CR-MI-Bz/ACAT-X samples with X larger than 10 demonstrate larger E_{corr} and lower I_{corr} compared to the neat ACAT or MI-Bz samples. The results indicate that blends of MI-Bz and ACAT could improve the performance of corrosion protection. As a result, the 3 samples, CR-MI-Bz/ACAT-20, CR-MI-Bz/ACAT-33, and CR-MI-Bz/ACAT-50 have protection efficiency greater than 90%, which is higher than the value recorded with the neat ACAT and MI-Bz samples. The best performance has been found with CR-MI-Bz/ACAT-33 which shows a protection efficiency of 98% and a corrosion rate of 4.8 $\mu\text{m y}^{-1}$. The value is about one order lower than that recorded with the neat ACAT sample and is better than the bare steel substrate by a factor of about 50. The above results suggest the synergistic effect of ACAT and MI-Bz on anticorrosion property. Moreover, the plots of the open-circuit potentials (OCP, vs SCE) as a function of the immersion time in the corrosive medium have been recorded CR-MI-Bz/ACAT-33-coated CRS sample (Figure 7b). The sample shows an initial OCP of -464 mV which decreases to -575 mV after a 90 min test. Meanwhile, the data recorded with ACAT-coated CRS sample is also shown in Figure 7b. The initial OCP and the OCP after 90-min immersion test of the sample is -646 and -771 mV, respectively. Compared to the ACAT-coated CRS sample, the CR-MI-Bz/ACAT-33-coated CRS sample shows relatively high OCP value and good OCP stability, both suggests that CR-MI-Bz/ACAT-33 could exhibit a better anticorrosion property that did ACAT. The enhanced anticorrosion efficiency of CR-MI-Bz/ACAT-33 has been attributed to its ability against diffusion of corrosive species for anticorrosion.³⁸ The function has been correlated to the water resistance of CR-MI-Bz/ACAT-33 to be discussed later.

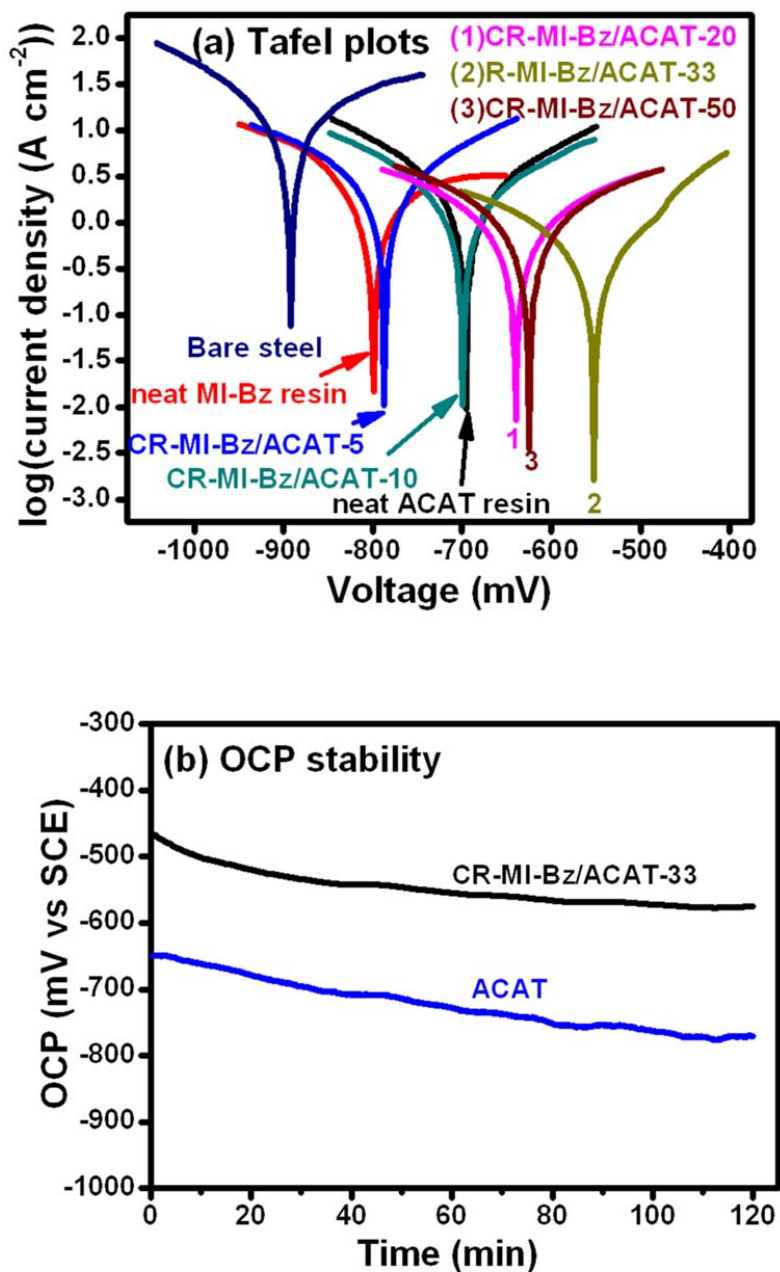


Figure 7. (a) Tafel plots of the thermally-cured resins of MI-Bz, ACAT, and their reactive blends. The voltages have been recorded vs SCE; (b) the plots of OCP stability in the corrosive medium recorded with ACAT-coated and CR-MI-Bz/ACAT-33-coated samples.

The high anticorrosion property of the CR-MI-Bz/ACAT-33 samples is further examined with an EIS at room temperature. The simple model has been utilized to analyze the data (Figure 8).^{37,38} As the Nyquist plots shown in Figure 8, the ACAT-coated CRS sample shows a charge transfer resistance (RCT) of about $96 \text{ k}\Omega \text{ cm}^2$, which is much higher than the value recorded for bare CRS ($2 \text{ k}\Omega \text{ cm}^2$). As a higher RCT value implies a better resistance performance and corresponds to a lower anticorrosion rate, the effect of ACAT coating on anticorrosion of CRS has been demonstrated. Moreover, the RCT value recorded with CR-MI-Bz/ACAT-33 further increases to $317 \text{ k}\Omega \text{ cm}^2$. Both of the results from EIS and Tafel analysis supports support to that the blend of MI-Bz and ACAT could demonstrate a high anticorrosion efficiency. The synergistic effect of ACAT and MI-Bz on anticorrosion property is further discussed below. As the neat ACAT shows an oxidation current and a reduction current of 52.8 and $70.5 \mu\text{A cm}^{-2}$, respectively and MI-Bz is not an electroactive material, the CR-MI-Bz/ACAT-X sample which possesses a higher ACAT content could exhibit a higher electroactivity. The experimental results support to the feature. The CR-MI-Bz/ACAT-X samples which contain ACAT contents high than 10 wt% exhibit electroactivity in the measurements (Figure 9). The function of ACAT as an active coating has also been reported and attributed to its electroactive property.^{39-42,49} On the other hand, the high water resistance and low water uptake of benzoxazine-based materials might contribute to the anticorrosion property.^{37,38} The water uptakes measured with the samples are collected in Figure 9b. The results indicate that the water uptakes increase with increasing the ACAT contents of the samples. Moreover, the neat ACAT resin also demonstrates a relatively high water diffusion rate (determined with the initial slope of the water absorption curve shown in Figure 9b) compared to the CR-MI-Bz/ACAT-X samples excepting CR-MI-Bz/ACAT-50.

The result indicates that the samples which have MI-Bz as the major component are water resistant. The electroactivity and water resistant property play counter roles for the anticorrosion property of the CR-MI-Bz/ACAT-X sample, so as to result in an optimum composition (33 wt% of ACAT) and the highest anticorrosion efficiency for the sample of CR-MI-Bz/ACAT-33.

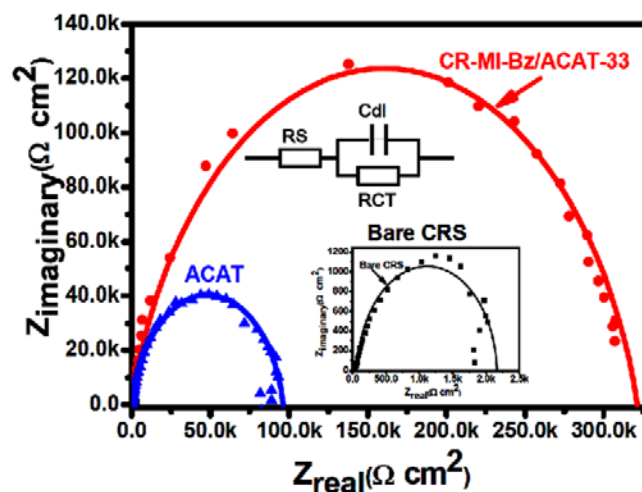


Figure 8. Nyquist plots for bare CRS and resin-coated samples. The equivalent circuit model used for analysis is included. RS: solution resistance, RCT: charge transfer resistance, Cdl: capacitance of the electrical double layer.

The adhesion ability of the anticorrosion material to the substrate is another critical issue for practical applications. The CR-MI-Bz/ACAT-X samples show good adhesion ability to the steel substrate after a knife-cutting test.⁴³ As shown in Figure 10, the cured samples coated on steel substrate after knife-cut do not show any cracks and fractions peeling off from the substrates. The hydrogen bonding between the -OH groups of the CRS surface and the cured resins contribute to the good interfacial adhesion. The -OH groups might also react with the maleimide group of MI-Bz to result in chemical linkages between the steel substrate and the resins,⁵⁰ which further enhance the adhesion ability of the resins to the steel substrate. In the test with an ATR-

FTIR (Figure 11), the decrease in the absorption intensity of the Fe-OH groups at about 3600-3650 cm^{-1} provides some support to the performance of the above mentioned reaction.⁵¹ Nevertheless, sufficient evidence to the formation of Fe-O-C linkages through the above-mentioned reaction between the substrate surface and the resin is not obtained due to serious overlap of the absorption peaks.

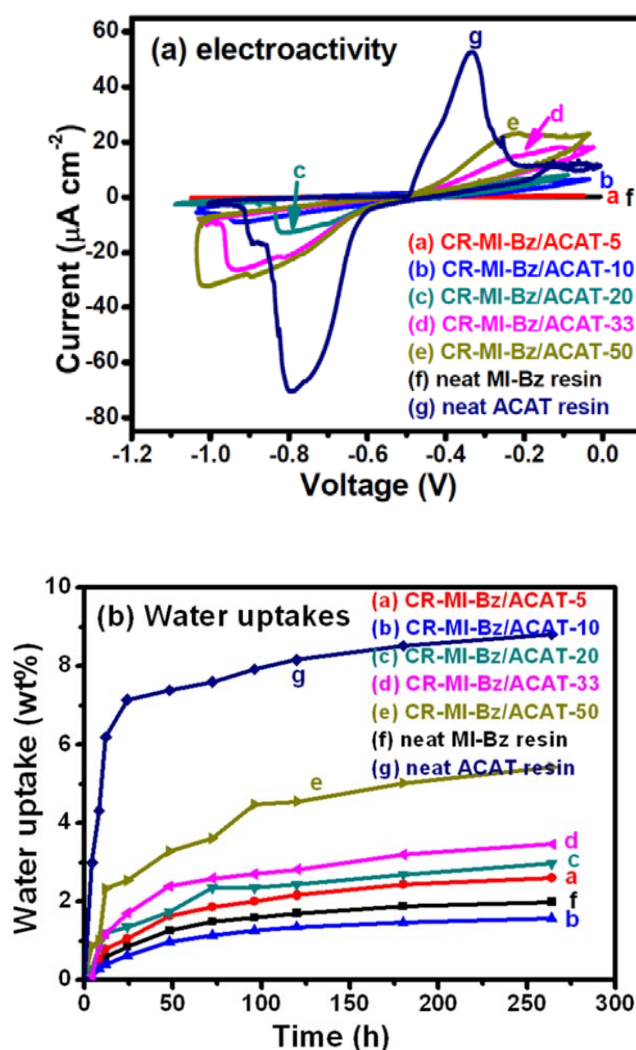


Figure 9. (a) Electroactivity and (b) water absorption tests on the thermally-cured resins of MI-Bz, ACAT, and their reactive blends. The curves in plot (a) were measured in a 3.5 wt% NaCl aqueous solution with a scan range from -1.1 to 0 V vs SEC at a scan rate of 100 mV min^{-1} .

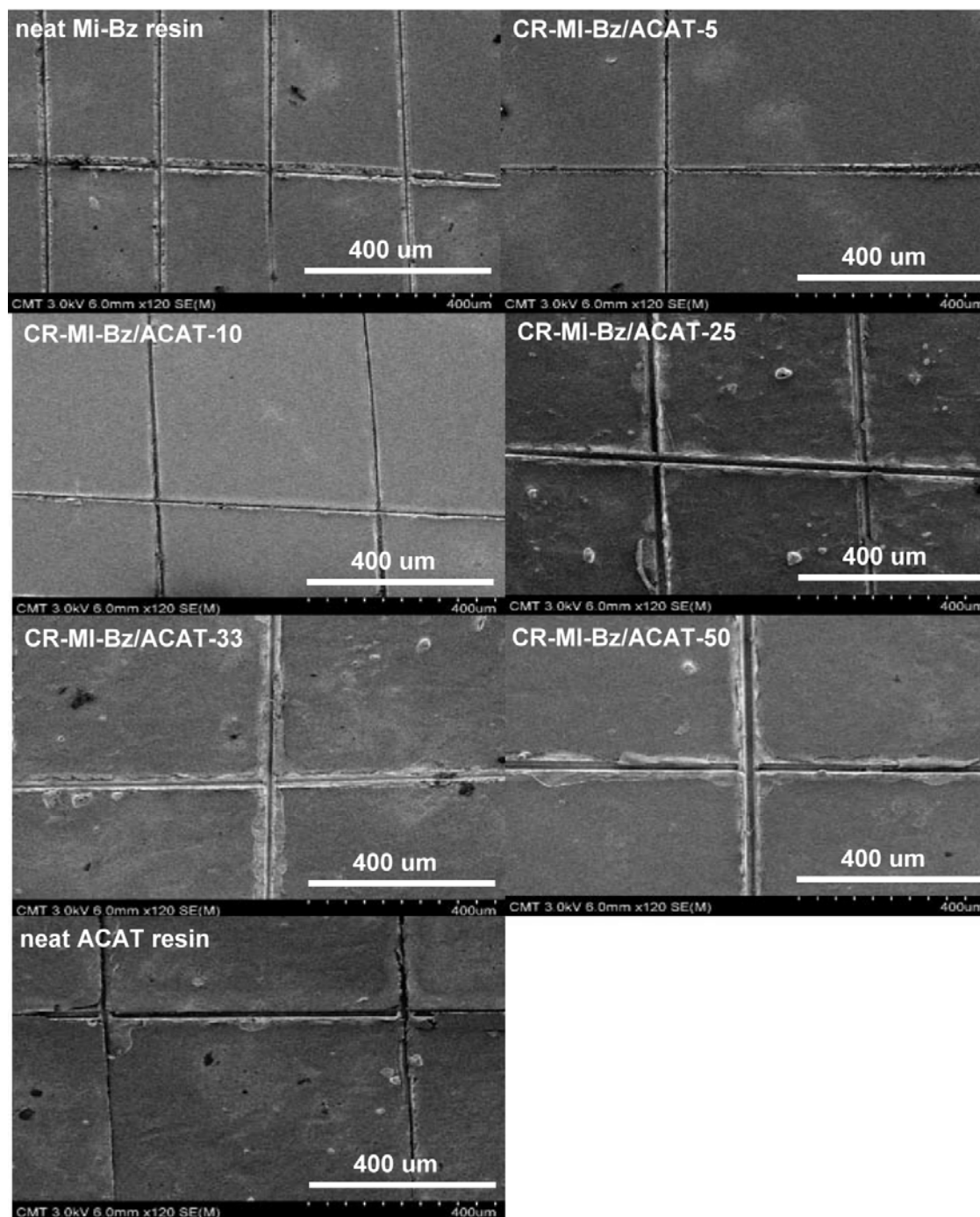


Figure 10. SEM micrographs of the knife-cut thermally-cured resins of MI-Bz, ACAT, and their reactive blends to present the adhesion tests on the samples.

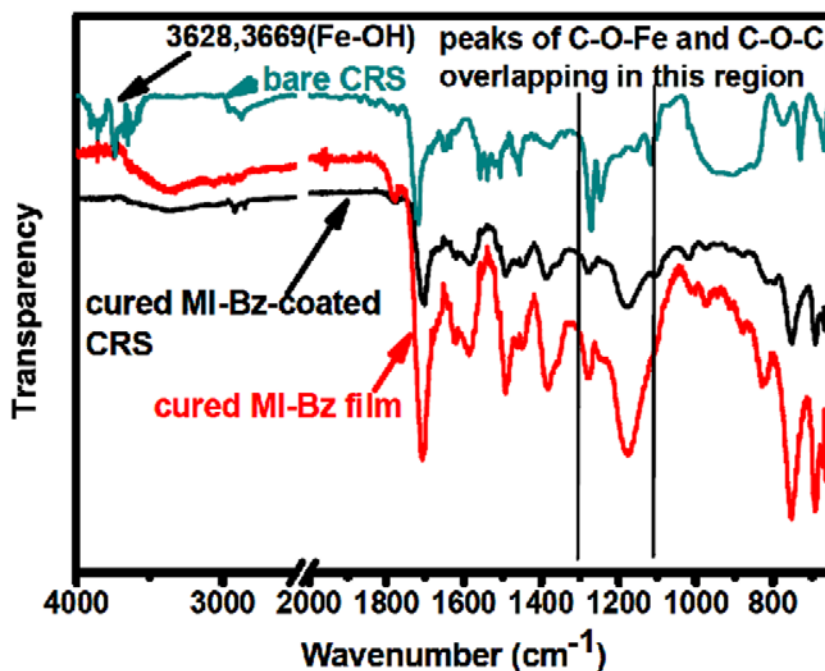


Figure 11. ATR-FTIR spectra recorded with the neat cured MI-Bz film, bare CS, and cured MI-Bz-coated CS samples.

4. Conclusion

The reactions of the reactive blends of MI-Bz and ACAT in a thermal processes have been illustrated to demonstrate that MI-Bz and ACAT are effective combination for preparation of high performance and functional thermosetting polymers. The thermally-cured CR-MI-Bz/ACAT resins exhibit good thermal stability and high flame retardancy. Moreover, a synergistic effect on anticorrosion has been observed with MI-Bz and ACAT, in which MI-Bz contributes water resistance and ACAT provides electroactivity to the effect. Consequently, the CR-MI-Bz/ACAT-33 sample has shown a protection efficiency of 98% and a corrosion rate of $4.8 \mu\text{m y}^{-1}$, which is about one order lower than that recorded with the neat ACAT sample. The prepared materials are highly potential for anticorrosion, flame-retardant, and thermally-stable coatings for metal protection.

Acknowledgement

The authors thank the Ministry of Science and Technology, Taiwan (NSC 102-2221-E-007-135-MY3) for financial support on this work.

Table 1. Thermal, mechanical, and flame retardant properties of the thermally-cured resins.

Sample	Dynamic mechanical analysis			Thermogravimetric analysis		
	Storage modulus at 50 °C (MPa)	T _g ^a (°C)	Storage modulus at 280°C (MPa)	T _d ^b (°C)	Char yield at 800 °C (wt%)	Calculated LOI ^c
Neat MI-Bz resin	2853	215	133	348	56	39.9
CR-MI-Bz/ACAT-5	3165	233	163	341	54	39.1
CR-MI-Bz/ACAT-10	3282	208	90	344	54	39.1
CR-MI-Bz/ACAT-20	2840	201	65	336	55	39.5
CR-MI-Bz/ACAT-33	2937	165	49	328	56	39.9
CR-MI-Bz/ACAT-50 ^d	-	-	-	322	51	37.9
Neat ACAT resin	5513	203	42	426	53	38.7

a. Determined with the peak of tanδ curves.

b. The temperature at 5 % weight loss.

c. Calculated from the char yield at 800 °C according to the van Krevelen's equation.

d. DMA data being not recorded with CR-MI-Bz/ACAT-50 due to sample cracks.

Table 2. Anticorrosion properties of the thermally-cured resins of MI-Bz and ACAT.

Sample	Water uptake (wt%)	Relative water diffusion rate	Redox behavior ($\mu\text{A cm}^{-2}$)		Electrochemical corrosion measurements			
			Oxidation	Reduction	E _{corr} (mV)	I _{corr} ($\mu\text{A cm}^{-2}$)	R _{corr} ($*10^{-2} \text{ mm y}^{-1}$)	E(%)
Neat MI-Bz resin	2.0	1.0	-	-	-800	1.96	3.8	84
CR-MI-Bz/ACAT-5	2.6	1.2	-	-	-778	1.88	3.64	84.66
CR-MI-Bz/ACAT-10	1.6	0.7	5.8	9.1	-722	1.63	3.16	86.7
CR-MI-Bz/ACAT-20	3.0	1.6	6.8	13.1	-608	0.76	1.47	93.8
CR-MI-Bz/ACAT-33	3.5	2.0	18.3	26.8	-570	0.25	0.48	97.96
CR-MI-Bz/ACAT-50	5.4	5.5	23.3	32.6	-625	0.88	1.71	92.82
Neat ACAT resin	8.8	8.4	53.0	70.2	-685	1.80	3.49	85.31
Bare steel	-	-	-	-	-892	12.25	23.7	-

REFERENCES

- (1) X. Ning, and H. Ishida, *J. Polym. Sci. Part A: Polym. Chem.*, **1994**, 32, 1121-1129.
- (2) N. N. Ghosh, B. Kiskan and Y. Yagci, *Prog. Polym. Sci.*, **2007**, 32, 1344-1391.
- (3) Y. L. Liu and C. I. Chou, *J. Polym. Sci. Part A: Polym. Chem.*, **2005**, 43, 5267-5282.
- (4) Y. L. Liu, C. W. Hsu and C. I. Chou, *J. Polym. Sci. Part A: Polym. Chem.*, **2007**, 45, 1007-1015.
- (5) Y. L. Liu, C. Y. Chang, C. Y. Hsu, M. C. Tseng, and C. I. Chou, *J. Polym. Sci. Part A: Polym. Chem.*, **2010**, 48, 4020-4026.
- (6) X. Wu, Y. Zhou, S. Z. Liu, Y. N. Guo, J. J. Qiu and C. M. Liu, *Polymer*, **2011**, 52, 1004-1012.
- (7) Q. C. Ran and Y. Gu, *J. Polym. Sci. Part A: Polym. Chem.*, **2011**, 49, 1671-1677.
- (8) H. C. Liu, W. C. Su and Y. L. Liu, *J. Mater. Chem.*, **2011**, 21, 7182 - 7187.
- (9) W. H. Hu, K. W. Huang and S. W. Kuo, *Polym. Chem.*, **2012**, 3, 1546-1554.
- (10) Y. Cheng, Y. Yang, D. Deng and F. Xiao, *Macromolecules*, **2012**, 45, 4085-4091.
- (11) M. Spontón, D. Estenoz, G. Lligades, J. C. Ronda, M. Galià, V. Cádiz, *J. Appl. Polym. Sci.*, **2012**, 126, 1369-1376.
- (12) C. Y. Hsieh, W. C. Su, C. S. Wu, L. K. Lin, K. Y. Hsu and Y. L. Liu, *Polymer*, **2013**, 54, 2945-2951.
- (13) Y. L. Liu, J. M. Yu and C. I. Chou, *J. Polym. Sci. Part A: Polym. Chem.*, **2004**, 45, 5954-5963.
- (14) A. Chernykh, T. Agag and H. Ishida, *Macromolecules*, **2009**, 42, 5121-5127.
- (15) T. Agag and T. Takeichi, *Macromolecules*, **2003**, 36, 6010-6017.
- (16) H. C. Chang, C. H. Lin, H. T. Lin and S. A. Dai, *J. Polym. Sci. Part A: Polym. Chem.*,

- 2012**, *50*, 1008-1017.
- (17) C. H. Lin, H. T. Lin, J. W. Sie, K. Y. Hwang and A. P. Tu, *J. Polym. Sci. Part A: Polym. Chem.*, **2010**, *48*, 4555-4566.
- (18) H. C. Chang, H. T. Lin and C. H. Lin, *Polym. Chem.*, **2012**, *3*, 970-978.
- (19) L. K. Lin, C. S. Wu, W. C. Su and Y. L. Liu, *J. Polym. Sci. Part A: Polym. Chem.*, **2013**, *51*, 3523-3530.
- (20) R. Kudoh, A. Sudo and T. Endo, *Macromolecules*, **2010**, *43*, 1185-1187.
- (21) M. Baqar, T. Agag, R. Huang, J. Maia, S. Qutubuddin and H. Ishida, *Macromolecules*, **2012**, *45*, 8119-8125.
- (22) S. Li and T. Zou, *J. Appl. Polym. Sci.*, **2012**, *123*, 922-928.
- (23) C. Zúñiga, G. Lligades, J. C. Ronda, M. Galià and V. Cádiz, *Polymer*, **2012**, *53*, 1617-1623.
- (24) H. Kimura, Y. Murata, A. Matsumoto, K. Hasegawa, K. Ohtsuka and A. Fukuda, *J. Appl. Polym. Sci.*, **1999**, *74*, 2266-2273.
- (25) T. Takeichi, Y. Guo and T. Agag, *J. Polym. Sci. Part A: Polym. Chem.*, **2000**, *38*, 4165-4176.
- (26) Y. L. Liu and J. M. Yu, *J. Polym. Sci. Part A: Polym. Chem.*, **2006**, *44*, 1890-1899.
- (27) T. Takeichi, Y. Saito, T. Agag, H. Muto and T. Kawauchi, *Polymer*, **2008**, *49*, 1173-1179.
- (28) X. Li and Y. Gu. *Polym. Chem.*, **2012**, *2*, 2778-2781.
- (29) C. H. Lin, S. J. Huang, P. J. Wang, H. T. Lin, and S. A. Dai, *Macromolecules*, **2012**, *45*, 7461-7466.

- (30) A. W. Kawaguchi, A. Sudo and T. Endo, *ACS Macro Lett.*, **2013**, *2*, 1-4.
- (31) A. A. Alhwaige, T. Agag, H. Ishida and S. Qutubuddin, *Biomacromolecules*, **2013**, *14*, 1806-1815.
- (32) J. Choi, K. M. Lee, R. Wycisk, P. N. Pintauro and P. T. Mather, *Macromolecules*, **2008**, *41*, 4569-4572.
- (33) H. Y. Li and Y. L. Liu, *J. Mater. Chem. A*, **2013**, *1*, 1171-1178.
- (34) C. F. Wang, Y. C. Su, S. W. Kuo, C. F. Huang, Y. C. Sheen and F. C. Chang, *Angew. Chem. Int. Ed.*, **2006**, *45*, 2248-2251.
- (35) C. S. Liao, C. F. Wang, H. C. Lin, H. Y. Chou and F. C. Chang, *Langmuir*, **2009**, *25*, 3359-3362.
- (36) T. H. Kao, J. K. Chen, C. C. Cheng, C. I. Su and F. C. Chang, *Polymer*, **2013**, *54*, 256-268.
- (37) C. Zhou, X. Lu, Z. Xin and J. Liu, *Corrosion Sci.*, **2013**, *70*, 145-151.
- (38) C. Zhou, X. Lu, Z. Xin, J. Liu and Y. Zhang, *Prog. Org. Coat.*, **2013**, *76*, 1178-1183.
- (39) Y. Wei, J. Wang, X. Jia, R. M. Yeh and P. Spellane, *Polymer*, **1995**, *36*, 4535-4537.
- (40) M. Fahlman, S. Jasty and A. J. Epstein, *Synth. Metals*, **1997**, *85*, 1323-1326.
- (41) K. Y. Huang, Y. S. Jhuo, P. S. Wu, C. H. Lin, Y. H. Yu and J. M. Yeh, *Eur. Polym. J.*, **2009**, *45*, 485-493.
- (42) K. Y. Huang, C. L. Shiu, P. S. Wu, Y. Wei, J. M. Yeh and W. T. Li, *Electrochim. Acta*, **2009**, *54*, 5400-5407.
- (43) C. W. Peng, K. C. Chang, C. J. Weng, M. C. Lai, C. H. Hsu, S. C. Hsu, Y. Y. Hsu, W. I. Hung, Y. Wei and J. M. Yeh, *Electrochim. Acta*, **2013**, *95*, 192-199.

- (44) Y. L. Liu, Y. J. Chen and W. L. Wei, *Polymer*, **2003**, *44*, 6465-6473.
- (45) Y. Wei, C. Yang and T. Ding, *Tetrahedron Lett.*, **1996**, *37*, 731-734.
- (46) X. Yang, Y. Jiang, T. Zhao and Y. Yu, *J. Appl. Polym. Sci.*, **2006**, *102*, 222-226.
- (47) C. S. Wu, S. H. Tsai and Y. L. Liu, *J. Polym. Sci. Part A: Polym. Chem.*, **2005**, *43*, 1923-1929.
- (48) D. W. van Krevelen, *Polymer*, **1975**; *16*, 615-620.
- (49) T. I. Yang, C. W. Peng, Y. L. Lin, C. J. Weng, G. Edgington, A. Mylonakis, T. C. Huang, C. H. Hsu, J. M. Yeh and Y. Wei, *J. Mater. Chem.*, **2012**, *22*, 15845-15852.
- (50) Z. Wang, Q. Ran, R. Zhu and Y. Gu, *J. Appl. Polym. Sci.*, **2013**, *129*, 1124-1130.
- (51) X. Song and J. F. Boily, *Phys. Chem. Chem. Phys.*, **2012**, *14*, 2579-2586.

Figure caption

Figure 1. Chemical structures and thermally-induced reactions of ACAT and MI-Bz.

Figure 2. DSC thermograms recorded on (a) MI-Bz/ACAT-5, (b) MI-Bz/ACAT-10, (c) MI-Bz/ACAT-20, (d) MI-Bz/ACAT-33, (e) MI-Bz/ACAT-50, (f) neat MI-Bz, and (g) neat ACAT samples.

Figure 3. Temperature-dependent FTIR spectra recorded on (a) MI-Bz/ACAT-33 and (b) MI-Bz/ACAT-50 at the heating process.

Figure 4. The reaction mechanism proposed for the thermally-induced curing reactions of MI-Bz/ACAT blends.

Figure 5. DMA thermograms recorded on the thermally-cured resins of MI-Bz, ACAT, and their reactive blends.

Figure 6. TGA thermograms recorded on the thermally-cured resins of MI-Bz, ACAT, and their reactive blends.

Figure 7. (a) Tafel plots of the thermally-cured resins of MI-Bz, ACAT, and their reactive blends. The voltages have been recorded vs SCE; (b) the plots of OCP stability in the corrosive medium recorded with ACAT-coated and CR-MI-Bz/ACAT-33-coated samples.

Figure 8. Nyquist plots for bare CRS and resin-coated samples. The equivalent circuit model used for analysis is included. RS: solution resistance, RCT: charge transfer resistance, Cdl: capacitance of the electrical double layer.

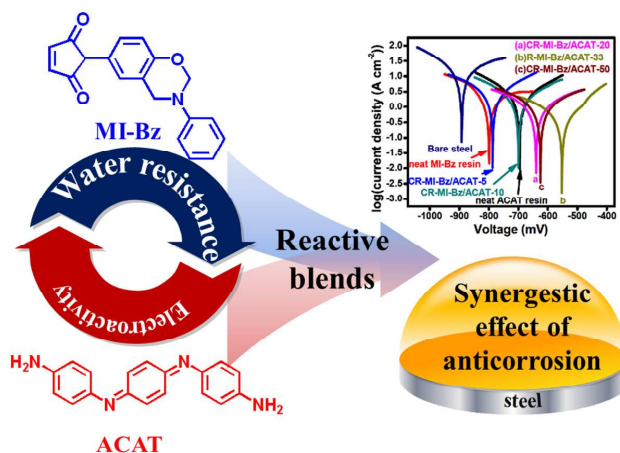
Figure 9. (a) Electroactivity and (b) water absorption tests on the thermally-cured resins of MI-Bz, ACAT, and their reactive blends. The curves in plot (a) were measured in a 3.5 wt% NaCl aqueous solution with a scan range from -1.1 to 0 V vs SEC at a scan rate of 100 mV min⁻¹.

Figure 10. SEM micrographs of the knife-cut thermally-cured resins of MI-Bz, ACAT, and their reactive blends to present the adhesion tests on the samples.

Figure 11. ATR-FTIR spectra recorded with the neat cured MI-Bz film, bare CS, and cured MI-Bz-coated CS samples.

Reaction Mechanism and Synergistic Anticorrosion Property of Reactive Blends of Maleimide-Containing Benzoxazine and Amine-Capped Aniline Trimer

Shin-Chen Lin, Chuan-Shao Wu, Jui-Ming Yeh, Ying-Ling Liu*



Reaction mechanism and synergistic effect on anticorrosion for reactive blends of a maleimide-containing benzoxazine and aniline trimer have been explored.